Electroconvection in nematic liquid crystals with positive dielectric and negative conductivity anisotropy

Á. Buka,[1] B. Dressel,[2] W. Otowski,[1,*] K. Camara,[3] T. Toth-Katona,[1] L. Kramer,[2] J. Lindau,[3] G. Pelzl,[3] and W. Pesch[2]
[1]*Research Institute for Solid State Physics and Optics, Hungarian Academy of Sciences, P.O. Box 49, H-1525 Budapest, Hungary*
[2]*Physikalisches Institut, Universität Bayreuth, D-95440 Bayreuth, Germany*
[3]*Institut für Physikalische Chemie, Martin-Luther-Universität, D-06099 Halle/Saale, Germany*
(Received 29 July 2002; published 26 November 2002)

Electroconvection in an unusual nematic compound with strongly positive dielectric anisotropy and negative anisotropy of the conductivity is investigated. For homeotropic alignment, where one has a direct transition to rolls or squares depending on the frequency of the applied voltage, we present a quantitative theory. From the comparison we infer values for some viscosities, which are rather unusual, but not unreasonable in view of the vicinity of the nematic-smectic transition. For planar alignment, electroconvection sets in above a splay Freedericksz transition with ''parallel rolls,'' which is also captured by the theory.

DOI: 10.1103/PhysRevE.66.051713 PACS number(s): 61.30.Gd, 47.54.+r, 47.20.Lz

I. INTRODUCTION

Nematic liquid crystals, the simplest type of intrinsically anisotropic fluids, continue to provide model systems for a wide variety of interesting nonlinear dynamical phenomena like optical instabilities [1], flow-induced nonlinear waves [2], critical properties of nonequilibrium transitions [3], and in particular electrically or thermally driven convection instabilities [3,4] (see also Ref. [5], and references therein). Whereas convection in nematics has so far contributed substantially to our general understanding of anisotropic pattern-forming systems, we present here in particular a direct transition to *isotropic convection*, which opens up scenarios unaccessible in simple fluids.

In nematics, the mean orientation of the rodlike molecules is described by the director $\hat{\mathbf{n}}$. The anisotropy is reflected in the material parameters such as the conductivity tensor $\sigma_{ij}=\sigma_\perp\delta_{ij}+\sigma_a n_i n_j$, where $\sigma_a=\sigma_\parallel-\sigma_\perp$ (and similarly the permittivity ϵ_{ij}). Here $\sigma_\parallel$ and $\sigma_\perp$ are the conductivities parallel and perpendicular to $\hat{\mathbf{n}}$, respectively. Electroconvection (EC) driven by an ac voltage $\sqrt{2}U\cos(\omega t)$ (effective amplitude U, frequency $\omega=2\pi f$) is commonly observed in nematics of positive conductive ($\sigma_a>0$) and negative dielectric anisotropy ($\epsilon_a<0$). Widely used and extensively studied examples from this class of materials are MBBA, *I*52, and Merck phases 4 and 5 [5], where experiments and theory match very well. In this paper we focus on EC for a new nematic with the combination of $\sigma_a<0$ and $\epsilon_a>0$, which has not been studied up to now (we are aware of one measurement carried out on a mixture, but the results are mostly unpublished [6]).

To appreciate a number of interesting features which will be described below, we first summarize some results of the conventional case $\sigma_a>0$ and, to start with, $\epsilon_a<0$. In this paper we restrict ourselves to the ''conduction regime,'' i.e., ω below the familiar cutoff frequency. In the well-studied *planarly* aligned cells ($\hat{\mathbf{n}}$ anchored parallel to the bounding plates leading to an axial anisotropy in the plane of the layer), convection sets in directly from the homogeneous state at the threshold $U_c(\omega)$. Slightly above onset, ordered roll patterns associated with a periodic director distortion characterized by the critical wave vector $\mathbf{q}_c(\omega)$ are found. The phenomenon can be described quantitatively by refined versions of the original Helfrich-Orsay theory (''standard model'') [4,7].

When decreasing σ_a (at $\epsilon_a<0$), U_c and $|\mathbf{q}_c|$ increase and diverge at $\sigma_a'/|\epsilon_a'|=|\alpha_2|/\eta_1-1(>0)$, where $\sigma_a'=\sigma_a/\sigma_\perp$, $\epsilon_a'=\epsilon_a/\epsilon_\perp$ and $\eta_1=(-\alpha_2+\alpha_4+\alpha_5)/2$. The material constants $\alpha_1,\ldots,\alpha_6$ are the Leslie viscosity coefficients [8,9]. When ϵ_a is increased and becomes positive, while the other material parameters are kept fixed, the EC threshold is eventually preceded by the spatially homogeneous splay Freedericksz transition, i.e., an equilibrium transition, which involves a distortion of the director field. The nonlinear aspects of the competition between EC and the Freedericksz transition have been of recent interest [10].

In contrast, for conventional materials ($\sigma_a>0$, $\epsilon_a<0$) with *homeotropic* alignment ($\hat{\mathbf{n}}$ anchored perpendicular to the bounding plates leading to an isotropic configuration), one can have a direct transition to EC only when ϵ_a' is near zero and $\alpha_3<0$ [4,11,12]. Then U_c is large and q_c is of order $(\alpha_2/\alpha_3)^{1/2}d^{-1}\gg 1$ (d is the sample thickness). We are aware of only one brief remark about an experimental observation [11]. For manifestly negative ϵ_a, there is first a bend Freedericksz transition, which spontaneously breaks the isotropy, followed by a transition to convection, driven by a mechanism very similar to that in planar cells [4,12]. The rolls, however, are disordered, which has recently led to extensive studies [13].

We now turn to the new case $\sigma_a<0$ and $\epsilon_a>0$. For *homeotropic* alignment, the possibility of a direct transition to EC has been hinted at in the early literature [9]. For *planar* alignment, a transition to EC can occur only after a splay Freedericksz transition, where a homeotropic layer develops in the bulk of the cell. (For completeness, we mention that for negative σ_a and ϵ_a, one does not expect a linear thresh-

*On leave from Institute of Physics, Cracow University of Technology, 30-084 Cracow, Poland.

old. There is, however, experimental evidence for EC via nonlinear effects [14].)

From the quantitative comparison between experiment and the linear and weakly nonlinear analysis we deduce some of the unknown material parameters. In particular, we find that α_1 is positive and large and α_3 is positive and larger than usual. Since conventional nematics have negative α_1 and very small α_3 (usually negative, i.e., flow aligning [8]), this appears surprising. However, as noted theoretically [15], as well as experimentally using the material 4-*n*-octyl-4′-cyanobiphenyl [16], and also in recent molecular dynamics simulations [17], α_1 and α_3 are expected to become positive and, in fact, to diverge near a second-order phase transition to a smectic phase. To our knowledge the present results represent the second experimental clue for this behavior (after the direct viscosity measurements of Ref. [16]).

II. EXPERIMENT

Our experiments were done in the nematic phase of a ''swallow-tailed'' compound, *p*-(nitrobenzyloxy)-biphenyl [18], which shows a phase sequence: isotropic-110 °C-nematic-94 °C-smectic-*C*-75 °C-smectic-*F*-(66.5 °C -smectic-*X*)-69 °C-crystalline. The structure of the monotropic (showing up only on cooling) smectic-*X* phase below the smectic-*F* has not been identified. The extended smectic-*C* (S_c) phase together with the direct transition to the nematic phase is presumably responsible for the negative conductivity anisotropy in the whole nematic range. Some material parameters such as the dielectric susceptibilities ($\epsilon_\parallel$ and $\epsilon_\perp$), conductivities ($\sigma_\parallel$ and $\sigma_\perp$), and the elastic constant (K_{11}) have been measured as a function of temperature.

EC measurements have been carried out at 96 °C. The temperature was controlled in an Instec hotstage with an accuracy of 0.05 °C. Samples with planar and homeotropic alignment using commercial ''EHC-Japan'' cells have been prepared with the nematic layer of thickness $d=11\pm1$ μm sandwiched between SnO_2 coated float glass plates (*x*-*y* plane) used as electrodes to apply the electric voltage across the sample (in the *z* direction). The patterns have been observed in a polarizing microscope and recorded by a charge-coupled device camera connected to a frame grabber card. Images have been digitized with a spatial resolution of 512×512 pixels and 256 grayscales.

III. HOMEOTROPIC ALIGNMENT

For *homeotropic alignment*, EC sets in directly from the undistorted state via a supercritical bifurcation in the whole conductive range up to its upper end at the cutoff frequency ω_{cut}. We found $\omega_{cut}\tau_q=0.7$, with the charge relaxation time $\tau_q=\epsilon_0\epsilon_\perp/\sigma_\perp$. For low frequencies, we observe a pattern of disordered rolls (stripes) at threshold. For high frequencies the rolls are replaced by squares. In the intermediate-frequency range, patches of rolls and squares ($R+S$, a mixture of the two patterns) appear [see Figs. 1(a–c)].

In the stripe patterns, one observes domain-wall-like lines along which the roll orientation abruptly changes, typical for the zigzag (ZZ) instability. The in-plane director (projection of the director onto the *x*-*y* plane) has been found experimentally to be perpendicular to the (local) roll direction. The difference in brightness and contrast in the different domains of Fig. 1(a) has a purely optical basis depending on the local angle between the director and the polarizer. Although the ZZ instability is characteristic for isotropic systems, this structure can rarely be observed under quasistationary conditions (see below) [19]. Occasionally, rolls at different angles were separated by an overlap region. Increasing the voltage the pattern breaks up into patches, but still does not exhibit the point defects typical for anisotropic convection. The ratio of areas with overlapping rolls and of parallel stripes increases with the frequency. No pure stripe regions can be observed above a critical frequency ω^*, with $\omega^*\tau_q=0.56$. Instead, we find square patterns [Fig. 1(c)], which retain near threshold some features of the ZZ character of the stripes, i.e., the lines making up the squares are undulated. We call this structure soft square pattern.

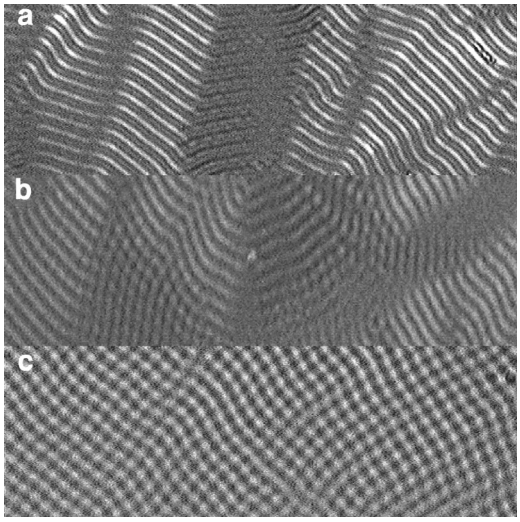

FIG. 1. Snapshots of sections of EC patterns near onset [$\epsilon=(U^2-U_c^2)/U_c^2=0.038$] for homeotropic alignment. ZZ rolls at $\omega\tau_q=0.1$ (corresponds to a physical size of 360 μm×110 μm) (a); rolls+squares at $\omega\tau_q=0.46$ (size 200 μm×65 μm) (b); and soft squares at $\omega\tau_q=0.65$ (size 120 μm×38 μm) (c).

A. Threshold behavior

Before presenting quantitative results, we discuss the qualitative features of the basic (Carr-Helfrich) destabilization mechanism. Starting from a (small) director distortion $n_x=n_{x0}\sin(qx)\cos(\pi z/d)$ about $\hat{\mathbf{n}}=\hat{\mathbf{z}}$, a space charge is generated by the charge focusing mechanism. The density of space charges (ρ_{el}) is obtained from the Poisson and charge conservation equations,

$$\nabla\cdot(\boldsymbol{\epsilon}\cdot\boldsymbol{\epsilon}_0\mathbf{E})=\rho_{el},\quad \nabla\cdot(\boldsymbol{\sigma}\cdot\mathbf{E}+\rho_{el}\mathbf{v})=-\partial_t\rho_{el}, \qquad (1)$$

where $\mathbf{v}$ denotes the velocity field. Linearizing around the homeotropic orientation and writing $\mathbf{E}=E_0\,\hat{\mathbf{z}}\cos(\omega t)-\nabla\varphi$, one easily obtains for the in-phase component of the charge density [the component $\sim\sin(\omega t)$ is not needed]

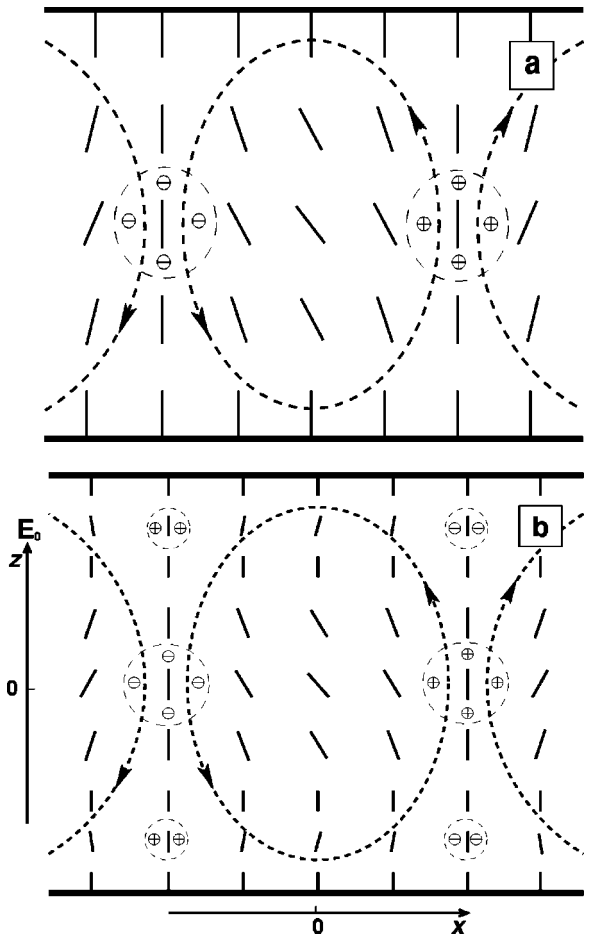

FIG. 2. Section of a convection roll pattern with the central roll covering the area $-\pi/(2q)\leqslant 0\leqslant \pi/(2q)$, $-d/2\leqslant z\leqslant d/2$ for homeotropic alignment: velocity field (short dashed) and director field $\mathbf{n}=(n_x,n_z)$. (a) $\alpha_3/|\alpha_2|=0.15$, (b) negligible torque contribution Γ_3 ($|\alpha_3/\alpha_2|\sim 0.01$). Also indicated are the space charge distributions at a time where the electric field points upward (otherwise the signs are reversed).

$$\rho_{el}=Q(q',\omega')qn_{x0}\,\sin(qx)\cos(\pi z/d)\epsilon_0 E_0\,\cos(\omega t),$$

$$Q(q',\omega')=-(\sigma_a'-\epsilon_a')\frac{\sigma(q')(1+q'^2)}{\sigma(q')^2+\omega'^2\epsilon(q')^2},$$

$$\epsilon(q')=1+\epsilon_a'+q'^2,\quad \sigma(q')=1+\sigma_a'+q'^2, \qquad (2)$$

with $q'=qd/\pi$, $\omega'=\omega\tau_q$. For our material with the Helfrich parameter, $\sigma_a'-\epsilon_a'<0$, i.e. $Q>0$, the space charge density ρ_{el} from Eq. (2) is related to the director distortion as indicated in Fig. 2(a) at a time where the electric field points upward. The flow generated by the Coulomb force $\langle\rho_{el}E_0\,\hat{\mathbf{z}}\cos(\omega t)\rangle$ (the symbol $\langle\cdot\rangle$ denotes the time average) is illustrated in Fig. 2(a). The velocity field $\mathbf{v}$ exerts on the director a torque $\Gamma_y=\Gamma_2+\Gamma_3$, where $\Gamma_2=-\alpha_2\partial_z v_x$, $\Gamma_3=-\alpha_3\partial_x v_z\sim\alpha_3 q'^2(\pi/d)v_x$ (the last estimate follows from the incompressibility condition). Clearly, Γ_2 reinforces the director distortion in most of the region (note that $\alpha_2<0$), which provides the positive feedback for the director distortion, and thus the destabilization of the homeotropic director orientation. Stabilizing mechanisms are provided by the dielectric torque on the director and the viscous damping of the flow. We note that in the usual nematics with $\sigma_a'-\epsilon_a'>0$, the hydrodynamic torque Γ_y would have to be reverted in order to have a direct transition to EC. This requires $\alpha_3<0$ and $q'^2\sim|\alpha_2/\alpha_3|\gg 1$.

In Figs. 3(a,b), the experimental results for the threshold voltage U_c and the critical wave vector q_c are shown as functions of $\omega\tau_q$. Also included are results from the linear stability analysis of the standard nematohydrodynamic description [9] evaluated by a numerical Galerkin procedure. We have measured and used for the calculations the material parameters $\epsilon_\perp=7.5$, $\epsilon_a=3.9$, $\sigma_a/\sigma_\perp=-0.65$, $K_{11}=9.5\times10^{-12}N$. The rest were chosen in order to get a good fit for $U_c(\omega)$, $q_c(\omega)$, which led to the ratio $K_{33}/K_{11}=2.5$ between *bend* and *splay* elastic constants, and $\alpha_1/|\alpha_2|=3.5$, $\alpha_3/|\alpha_2|=0.15$, $\eta_1/|\alpha_2|=1.06$, and $\eta_2/|\alpha_2|=0.21$ for the viscosity constants [20]. The large α_1 and positive α_3 were necessary to obtain the correct low-frequency threshold

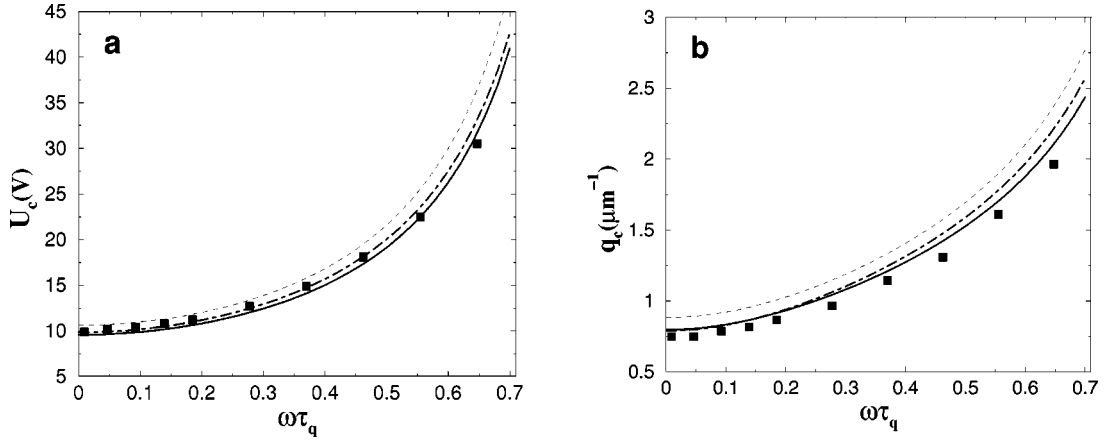

FIG. 3. Comparison between experimental (solid squares) and theoretical threshold voltage (a) and the corresponding critical wave number (b) vs dimensionless frequency. Solid line represents rigorous Galerkin expansion; dot-dashed line represents two-mode formula [cf. Eq. (3)], and the dashed represents one-mode formula [$M(q')\equiv 0$ in Eq. (3)].

and the quite strong increase (in comparison to the conventional $\sigma_a>0$ case) of q_c vs ω. The effective viscosities $\eta_1=(-\alpha_2+\alpha_4+\alpha_5)/2$, $\eta_2=(\alpha_3+\alpha_4+\alpha_6)/2$, and $\eta_3=\alpha_4/2$ correspond to flow geometries with $\hat{\mathbf{n}}$ parallel to the flow gradient, the flow velocity, and the vorticity, respectively (α_1 comes in only when $\hat{\mathbf{n}}$ is aligned obliquely [9]).

In the assessment of the parameters, we were guided by an analytic approximation for the neutral curve $U_0(q)$ [with the minimum $U_c=U_0(q_c)$] obtained from a Galerkin expansion with two z modes for the charge density and the director (e.g., $n_x\sim[\cos(\pi z/d),\cos(3\pi z/d)]$) and one time-Fourier mode.

$$U_0^2=\frac{K_{33}\pi^2}{\epsilon_0\epsilon_\perp}\frac{2q'^2}{S_1+S_2+\sqrt{(S_1-S_2)^2+M}}, \tag{3}$$

$$S_1=\frac{1}{1+k_1q'^2}\left[I_hQ(q')\frac{\alpha_2-\alpha_3q'^2}{\eta_h(q')}-\epsilon_a^{eff}(q')\right],$$

$$S_2=\frac{1}{1+k_1q'^2/9}\left[I_h'Q(q'/3)\frac{\alpha_2-\alpha_3q'^2/9}{\eta_h(q')}-\epsilon_a^{eff}(q'/3)\right],$$

$$M=\frac{4I_hI_h'(\alpha_2-\alpha_3q'^2)(\alpha_2-\alpha_3q'^2/9)Q(q')Q(q'/3)}{(1+k_1q'^2)(1+k_1q'^2/9)\,\eta_h^2(q')},$$

$$\epsilon_a^{eff}(q')=q^2\epsilon_a'\frac{[\sigma(q')(1+\sigma_a')+\omega'^2\epsilon(q')(1+\epsilon_a')](1+q^2)}{\sigma(q')^2+\omega'^2\epsilon(q')^2},$$

$$\eta_h(q')=\eta_2+(\eta_1+\eta_2+\alpha_1)I_1q'^{-2}+\eta_1\lambda_1^4q'^{-4},$$

where $k_1=K_{11}/K_{33}$, and $I_h=0.972\,67$, $I_h'=0.026\,056$, $I_1=1.246\,52$, $\lambda_1=1.505\,62$ are projection integrals. The results of the two-mode formula are included in Figs. 3(a,b) (dash-dotted) as well as the one-mode approximation obtained from Eq. (3) by setting $M(q')=0$ (dashed), resulting in $U_0^2\sim S_1^{-1}$.

The one-mode formula, which captures already the crucial mechanisms, has been given before [5,12] without reference to its applicability for $\sigma_a<0$. In the expressions for $S_1(q')$ [and $S_2(q')$], one recognizes the mechanisms discussed above: the driving mechanism proportional to $Q(q')(\alpha_2-\alpha_3q'^2)$ and stabilizing effects included in the effective shear viscosity $\eta_h(q')$ and the dielectric torque $\sim\epsilon_a^{eff}(q')$ (the complexity of this expression arises from the field distortion $-\nabla\phi$).

The torque contributions Γ_2 and Γ_3 along a vertical cut through the roll center ($x=0$ in Fig. 2) are shown in Fig. 4 for our case with a comparatively large α_2 and not too small value for $\alpha_3/|\alpha_2|=0.15$. They are both symmetric in z. Γ_2 has extrema of opposite sign at the center ($z=0$) and at the boundaries ($z=\pm d/2$). Γ_3 has its maximum at the center and is zero at the boundaries. A director configuration as described by the one-mode approximation [$n_x(z)\sim\cos(\pi z/d)$], i.e., maximal at the center, zero at the boundaries, and no sign change is not adapted well to the torque Γ_2 (see Fig. 4, curve *I*). Thus, if Γ_2 dominates, the one-mode approximation is not satisfactory and the resulting thresholds are overestimated considerably. This would be the case for the usual materials where $\alpha_3/|\alpha_2|$ is very small. Including the second mode [Fig. 2(b) and curve *II* in Fig. 4] resolves this problem and leads to an excellent approximation for q_c, U_c. In our case $\alpha_3q'^2/|\alpha_2|$ is, in fact, appreciable, and Γ_3 reinforces $\Gamma_2(z)$ in the central region. Then already the one-mode approximation captures the dominant effects. This is also the case in conventional planar EC with $\sigma_a>0$, where the roles of α_2 and $-\alpha_3$ are interchanged.

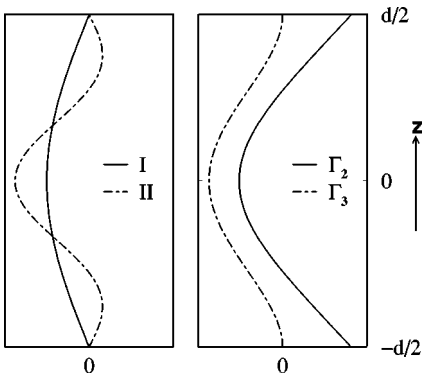

FIG. 4. Sketch of vertical cuts through the center of a convection roll ($x=0$) for homeotropic alignment (arbitrary units). Left panel represents in-plane director n_x in Figs. 2(a) (solid) and 2(b) (dashed). Right panel represents torque contributions Γ_2 and Γ_3.

Interestingly, the homeotropic one-mode ($M=0$) threshold formula (3) goes over into the planar one-mode formula relevant for $\sigma_a>0$, $\epsilon_a<0$ [4] if one interchanges the subscripts $\|\leftrightarrow\perp$ and the material parameters $K_{11}\leftrightarrow K_{33}$, $\eta_1\leftrightarrow\eta_2$, $\alpha_2\leftrightarrow-\alpha_3$. These correspondences occur naturally when switching the boundary conditions between homeotropic and planar.

Actually, in the homeotropic geometry, the effective viscosity is relatively large, which explains why the threshold is higher than in the planar geometry (see below). The strong damping effect of the dielectric torque resulting from the large value of ϵ_a is also responsible for the relatively low cutoff $\omega_{cut}\tau_q=0.7$.

B. Nonlinear range

Penetrating into the nonlinear regime (increasing the voltage above threshold), we observe at low frequencies a gradual decrease of the size of the patches and acceleration of the dynamics, and thereby a continuous transition into the chaotic state. At high frequencies (above ω^*), on the other hand, the soft square pattern undergoes a broad transition ending in a crystal-like, rigid, almost perfect, quadratic lattice which we call hard-square pattern with sharp boundaries between differently oriented domains (see Fig. 5). Hard-square domains coarsen with time and do not qualitatively change with the voltage up to a critical value where they undergo a discontinuous transition to chaos. The hard-square pattern occurs also below ω^* down to $\omega\tau_q=0.34$ where the

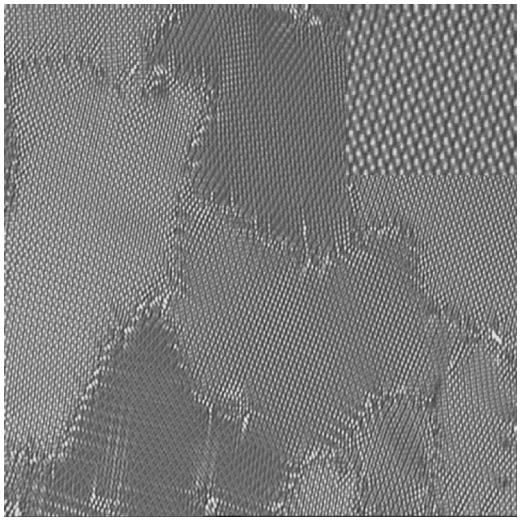

FIG. 5. Snapshot of a section of hard square patterns at $\omega\tau_q = 0.53$ and $\epsilon = 0.81$. (size 330 μm$\times$330μm). The inset shows a two times enlargemented section of size 55 μm$\times$55 μm.

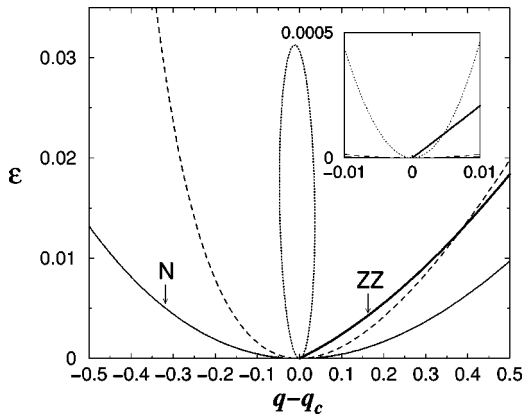

FIG. 6. Stability diagram from a weakly nonlinear calculation slightly below the transition point ω^*_{theo} to squares. Above the neutral curve (N, thin solid line), the Eckhaus (dashed) and ZZ instability (ZZ, thick solid) are shown. Outside the elongated bubble in the center rolls are cross roll unstable. The region $(q-q_c, \epsilon)\approx 0$ is enlarged in the inset.

transition line merges with the onset of chaos. A more detailed study of the square patterns (soft and hard) is under way.

We have also performed a numerical stability analysis of the roll solutions in the weakly nonlinear regime (see Fig. 6). With the above parameters, we find that the transition to rolls is replaced by a transition to squares above $\omega^*_{theo}\tau_q = 0.6$, which correlates well with the experimentally observed crossover to squares at $\omega^*\tau_q = 0.56$. The instability arises when the Landau coefficient g_s describing saturation of the roll amplitude at cubic order becomes larger than the coefficient g_{cr} describing the interaction between the two roll systems with orthogonal wave vectors. Both coefficients grow with increasing frequency due to the growing effect of viscosity. However, the increase is stronger for g_s because for the two-dimensional velocity field the adverse viscosity effects are particularly large. In Fig. 6 we show a stability diagram in the ϵ, q plane for a frequency slightly below ω^*_{theo}. Note the narrow cross roll stable range which shrinks to zero above $\omega^*_{theo}\tau_q$.

Squares at the onset are also observed in Rayleigh-Bénard convection in the presence of boundary plates with finite heat conductivity, consistent with the theory (see, e.g., Refs. [21,22]). Recently, also square patterns with a subsequent (secondary) transition to rolls have been found in Bénard-Marangoni convection [23], although this is not supported by theory [24]. One actually has expected subcritical hexagons at threshold, which is excluded in our case for symmetry reasons. Our system is unique in the sense that the transition from rolls to squares at threshold can be easily induced by varying the frequency as secondary control parameter.

Moreover, we find that in the roll regime the long-wavelength ZZ instability [25] destabilizes rolls already at onset, since the ZZ line, which emerges from the point U_c, q_c (this is generic for isotropic systems [26]) is tilted with a strong slope to the right (see Fig. 6). This, together with the fact that the ZZ instability is generally of supercritical nature [27], explains the experimentally found ZZ patterns [see Fig. 1(a)]. Such effects would be difficult to observe in the Rayleigh-Bénard convection in simple fluids,

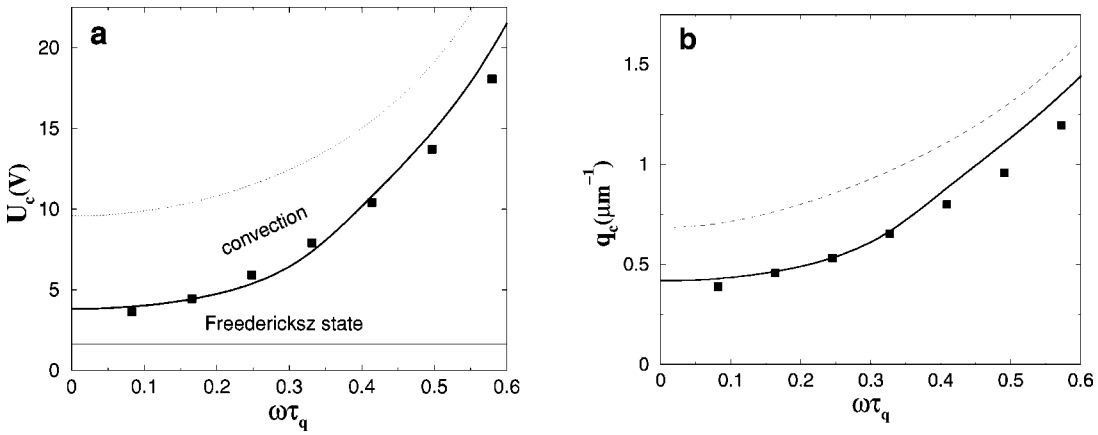

FIG. 7. Planar alignment, showing the comparison of experiment (filled squares) and linear theory (solid line) for the onset of convection. Dotted lines show theoretical curves for homeotropic alignment. Threshold voltage vs frequency (a) and wave number vs frequency (b).

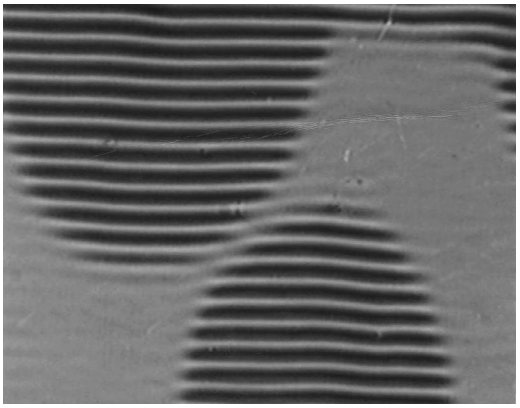

FIG. 8. Planar alignment, showing a representative snapshot after a jump to $\epsilon=0.2$, and showing fronts that move in (size 260 μm$\times$200 μm).

where the ZZ line tilts to the left (except in the large Prandtl number case, where it is essentially vertical [25]). Both slopes result mainly from mean-flow effects, which have opposite signs for the two systems [28]. In isotropic systems, the advection term $(\mathbf{v}\cdot\boldsymbol{\nabla})\,\mathbf{v}$ is responsible for the mean flow, whereas in nematics the anisotropic viscous terms give the main contribution [28].

Studies on coupled amplitude equations show that squares suffer the same types of long-wave instabilities as rolls. In particular, one expects the ZZ instability to persist in the square regime [27], and this appears to be the reason for the undulations of the soft squares near threshold (see Fig. 1). A detailed discussion of the weakly nonlinear properties will be given elsewhere.

IV. PLANAR ALIGNMENT

For *planar alignment* $\mathbf{n}=\hat{\mathbf{x}}$, one first has a splay Fréedericksz transition at a critical voltage $U_{F1}=1.6$ V where the director starts turning into the z direction. Experimentally, we find that EC sets in on the homogeneously distorted state at a voltage which, for low frequency, is about 40% of the threshold in the homeotropic case. For increasing frequency, the ratio moves towards 1. Well-aligned rolls appear at the threshold [see Fig. 10(a)] in the whole frequency range, like that in ordinary anisotropic EC, however, with orientation *parallel* to the director alignment, contrary to *normal rolls* in ordinary EC. The wave number is at low frequency, about 50% smaller than in the homeotropic case. It scales with d^{-1}, as has been checked for samples with thicknesses in the range of 4–50 μm.

Figures 7(a,b) show the critical voltage and wave number at the onset as a function of the frequency. Continuous lines are theoretical curves calculated on the basis of a linear stability analysis of the Fréedericksz state, using the material parameters from the homeotropic fit. (For comparison, dotted lines indicate the theoretical curves of the direct transition to EC for the homeotropic alignment.)

Due to the Fréedericksz-distorted ground state, the theoretical analysis is more tedious than in the homeotropic case. Since the critical voltage U_c for onset of EC is considerably

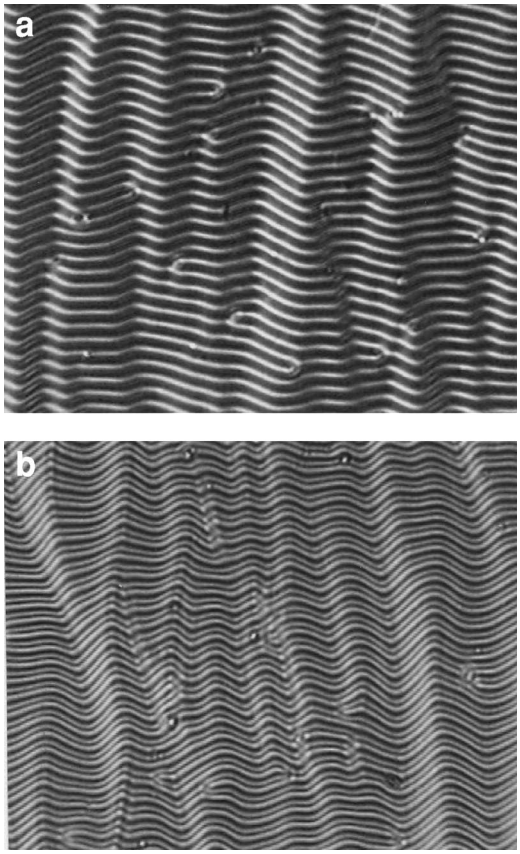

FIG. 9. Snapshot of ZZ modulated parallel rolls in planar alignment at $\omega\tau_q=0.32$ and two different ϵ; (a) $\epsilon=0.30$, (b) $\epsilon=1.04$ (size of both pictures: 260 μm$\times$200 μm).

higher than U_{F1}, the Fréedericksz distortion is strong ($n_z\approx 1$ in the midplane) when EC sets in and there are strongly distorted boundary layers. To resolve the boundary layers in the numerical Galerkin analysis, at least 8 z modes (Tchebyshev polynomials) are required. Keeping two time-Fourier modes results in a good quantitative fit to the experimental points (especially for the low-frequency range), which provides an additional argument for the correctness of the parameters taken from the homeotropic case. For $\omega\tau_q<0.4$, the analysis confirms the parallel rolls (roll axis in the x direction), whereas for $\omega\tau_q>0.4$, normal rolls have a slightly lower threshold. This slight discrepancy with the experiments could not be resolved by using more z modes.

We have not followed up this discrepancy because at this time the nature of the bifurcation is unclear. In the experiments one can identify a jump in the contrast, although we did not find hysteresis (if any, it should be less, than 0.01 V, the measuring uncertainty). The transition is mediated by fronts as demonstrated in Fig. 8. The snapshot shows patterning fronts traveling inward after an increase of the voltage. However, there are indications that a low-contrast pattern arises already at voltages slightly before the jump. At this time, we cannot exclude the possibility that this is due to a memory effect from previous runs. Possibly, the strong torques in the boundary layers can impose a long-lasting imprint in the surface anchoring properties, which could lead to the type of precursor observed. A preliminary weakly non-

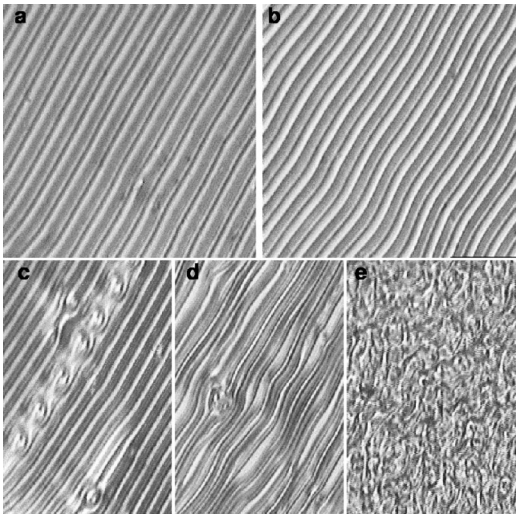

FIG. 10. Snapshots of EC patterns in planar alignment with increasing ϵ at $\omega\tau_q=0.05$; (a) parallel rolls ($\epsilon=0.17$), (b) ZZ rolls ($\epsilon=1.07$), (c) ''running bubbles'' ($\epsilon=3.45$), (d) stripe domains ($\epsilon=4.45$), and (e) chaos ($\epsilon=8.8$). Size of (a), (b): 225 μm$\times$225 μm; size of (c), (d), (e): 150 μm$\times$225 μm.

linear analysis exhibits a bifurcation, which at low frequencies is weakly supercritical. Rather small changes of the parameters or additional effects not included in the standard theory (e.g., flexoelectricity and weak-electrolyte effects) could change this into a subcritical bifurcation.

Increasing the voltage in the experiments, the parallel rolls persist in some ϵ range before they become ZZ modulated (see Fig. 9). Further above, a transition to ''stripe domains'' occurs, which consist of elongated domains of a thickness of several rolls running parallel with the rolls. This is followed by the transition to chaos. In addition, below $\omega\tau_q=0.1$, we detect in the ϵ range between the ZZ rolls and stripes a dynamic state with round shaped bubbles, isolated or several in a row, running along the rolls. Snapshots of the above structures are shown in Figs. 10(a–e) for $\omega\tau_q=0.05$. A comprehensive experimental voltage-frequency phase diagram is presented in Fig. 11.

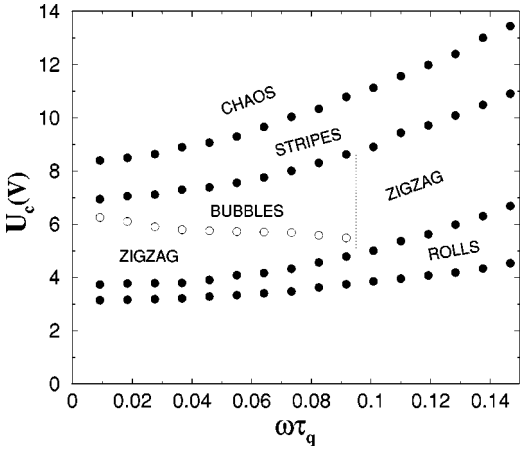

FIG. 11. Experimental voltage-frequency phase diagram for planar alignment.

V. CONCLUDING REMARKS

In conclusion, we have demonstrated that EC can occur even for materials with large positive dielectric anisotropy, provided the anisotropy of the conductivity is negative. For homeotropic alignment one has a direct transition to EC, whereas for planar alignment, EC occurs above a Fréedericksz transition. The scenario of patterns observable in the homeotropic case is distinct from that found in thermal convection of isotropic fluids. The comparison with theory has allowed us to infer material parameters that are difficult to measure directly. The signs and values of α_1 and α_3 turn out to be unconventional, although admissible in view of the vicinity of the nematic-smectic transition.

ACKNOWLEDGMENTS

We wish to thank N. Eber for illuminating discussions. Financial support through Grant Nos. OTKA-T031808, EU-RTN (PHYNECS), and EU ICA1-CT-2000-70029 is gratefully acknowledged.

[1] F. Simoni, *Nonlinear Optical Properties of Liquid Crystals* (World Scientific, Singapore, 1997); G. Demeter, Phys. Rev. E **61**, 6678 (2000).

[2] T. Börzsönyi, A. Buka, A.P. Krekhov, O.A. Scaldin, and L. Kramer, Phys. Rev. Lett. **84**, 1934 (2000).

[3] M.A. Scherer, G. Ahlers, F. Hörner, and I. Rehberg, Phys. Rev. Lett. **85**, 3754 (2000).

[4] L. Kramer and W. Pesch, in *Physical Properties of Nematic Liquid Crystals*, edited by D.A. Dunmur, A. Fukuda, and G.R. Luckhurst, Emis Datareview Series No. 25 (INSPEC, London, 2001), Vol. I, p. 441, and references therein.

[5] *Pattern Formation in Liquid Crystals*, edited by A. Buka and L. Kramer (Springer-Verlag, New York, 1996).

[6] M. Bock, G. Heppke, E.-J. Richter, and F. Schneider, Mol. Cryst. Liq. Cryst. **45**, 221 (1978).

[7] Within the standard model, flexoelectricity and electrolyte effects are neglected. Under most circumstances this is justified.

[8] F.M. Leslie, in *Theory and Applications of Liquid Crystals*, edited by J.L. Ericksen and D. Kinderlehrer (Springer-Verlag, New York, 1987).

[9] P.G. de Gennes and J. Prost, *The Physics of Liquid Crystals* (Clarendon Press, Oxford, 1993).

[10] A. Hertrich, W. Pesch, and J.T. Gleeson, Europhys. Lett. **34**, 417 (1996).

[11] M.I. Barnik, L.M. Blinov, M.F. Grebenkin, S.A. Pikin, and V.G. Chigrinov, Sov. Phys. JETP **42**, 550 (1976).

[12] A. Hertrich, W. Decker, W. Pesch, and L. Kramer, J. Phys. II **2**, 1915 (1992).

[13] J.-H. Huh, Y. Hidaka, and S. Kai, Phys. Rev. E **58**, 7355

(1998); P. Toth, A. Buka, J. Peinke, and L. Kramer, *ibid.* **58**, 1983 (1998); A.G. Rossberg, N. Eber, A. Buka, and L. Kramer, *ibid.* **61**, R25 (2000).

[14] M. Goscianski and L. Léger, J. Phys. (Paris) **36**, C1-231 (1975); H.R. Brand, C. Fradin, P.L. Finn, W. Pesch, and P.E. Cladis, Phys. Lett. A **235**, 508 (1997).

[15] F. Jähnig and F. Brochard, J. Phys. (Paris) **35**, 301 (1974).

[16] H. Kneppe, F. Schneider, and N.K. Sharma, J. Chem. Phys. **77**, 3203 (1981); Ber. Bunsenges. Phys. Chem. **85**, 784 (1981).

[17] L. Bennett and S. Hess, Phys. Rev. E **60**, 5561 (1999).

[18] U. Emmerling, S. Diele, H. Schmalfuss, J. Werner, H. Kresse, and J. Lindau, Macromol. Chem. Phys. **199**, 1529 (1998).

[19] C. Bowman, T. Passot, M. Assenheimer, and A.C. Newell, Physica D **119**, 250 (1998).

[20] The linear behavior depends only on the ratio of the viscosity constants. Thus the knowledge of α_2 that is typically of the order of 10^{-1} Ns/m^2. In the nonlinear regime, an additional dependence $Q=\tau_d/\tau_q$ with the director relaxation time $\tau_d=\alpha_2 d^2/(K_{33}\pi^2)\gg 1$ comes into play. However, in the limit of large $Q\approx 10^3$ as in our case, this dependence can be neglected. Furthermore, the location of the codimension-2 point ω^* depends also on the unknown *twist* constant K_{22}. With the choice $K_{22}/K_{11}=0.53$ comparable to the corresponding value in phase 5, the experimental and the theoretical location of the codimension-2 point matched satisfactorily.

[21] P. Le Gal and V. Croquette, Phys. Fluids **31**, 3440 (1988).

[22] M. Westerburg and F. Busse, J. Fluid Mech. **432**, 351 (2001).

[23] W.A. Tokaruk, T.C.A. Molteno, and S.W. Morris, Phys. Rev. Lett. **84**, 3590 (2001).

[24] A. Engel and J.B. Swift, Phys. Rev. E **62**, 6540 (2001).

[25] A. Schlüter, D. Lortz, and F.H. Busse, J. Fluid Mech. **23**, 129 (1965); F.H. Busse and R.M. Clever, *ibid.* **91**, 319 (1979).

[26] A.C. Newell and J.A. Whitehead, J. Fluid Mech. **28**, 279 (1969).

[27] R. B. Hoyle, in *Time-Dependent Convection*, edited by Peter A. Tyvand (Computational Mechanics Publications, Southampton, 1998), p. 51.

[28] E. Plaut and W. Pesch, Phys. Rev. E **59**, 1747 (1998).